

# In situ high-pressure single-crystal X-ray study of aegirine, $\text{NaFe}^{3+}\text{Si}_2\text{O}_6$ , and the role of M1 size in clinopyroxene compressibility

ANDREW C. MCCARTHY,<sup>1,\*</sup> ROBERT T. DOWNS,<sup>1</sup> RICHARD M. THOMPSON,<sup>1</sup>  
AND GÜNTHER J. REDHAMMER<sup>2</sup>

<sup>1</sup>Department of Geosciences, University of Arizona, Tucson, Arizona 85721-0077, U.S.A.

<sup>2</sup>Department of Materials Engineering and Physics, Division of Mineralogy, University of Salzburg, Hellbrunnerstrasse 34, A-5020 Salzburg, Austria

## ABSTRACT

The crystal structure of a synthetic aegirine crystal,  $\text{NaFe}^{3+}\text{Si}_2\text{O}_6$ , was studied at room temperature, under hydrostatic conditions, over the pressure range 0–11.55 GPa using single-crystal X-ray diffraction. Unit-cell data were determined at 16 pressures, and intensity data were collected at eight of these pressures. A third-order Birch-Murnaghan equation of state fit to the  $P$ - $V$  data from 0–11.55 GPa yielded  $K_0 = 117(1)$  GPa,  $K'_0 = 3.2(2)$ , and  $V_0 = 429.40(9)$  Å<sup>3</sup>. Aegirine, like the other Na-clinopyroxenes that have been examined at high pressure, exhibits strongly anisotropic compression, with unit strain axial ratios  $\epsilon_1:\epsilon_2:\epsilon_3$  of 1.00:2.38:2.63. Silicate chains in aegirine become more O-rotated with pressure, reducing  $\angle\text{O3-O3-O3}$  from 174.1(1)° at ambient pressure to 165.5(5)° at 10.82 GPa. No evidence of a phase transition was observed over the studied pressure range. The relationship between M1 cation radius and bulk modulus is examined for 14 clinopyroxenes, and two distinct trends are identified in a plot of these values. The distinction between these trends can be explained by the presence or absence of antipathetic bonds around M2, a feature first described by McCarthy et al. (2008). Aegirine, with  $\text{Fe}^{3+}$ , has nearly the same bulk modulus, within error, as hedenbergite, with  $\text{Fe}^{2+}$ , despite the difference in M2 bonding topology, M2 (Fe) valence and ambient unit-cell volume. Several explanations for this apparent paradox are considered.

**Keywords:** Aegirine, crystal structure, high pressure, single-crystal X-ray diffraction, clinopyroxene, compressibility, elasticity, bulk modulus

## INTRODUCTION

This study examines the relationship between M1 chemistry and compressibility in  $C2/c$  and  $P2_1/c$  silicate clinopyroxenes. Many such pyroxenes have been subjected to high-pressure single-crystal X-ray diffraction studies (Hugh-Jones and Angel 1994; Hugh-Jones et al. 1997; Zhang et al. 1997; Arlt et al. 1998; Yang et al. 1999; Arlt and Angel 2000; Hattori et al. 2000; Tribaudino et al. 2000; Origlieri et al. 2003; Gatta et al. 2005; Bindi et al. 2006; Downs and Singh 2006; Nestola et al. 2006; McCarthy et al. 2008; Thompson and Downs 2008). We examine data for 14 pyroxenes: aegirine (this study) plus 13 from the literature. First-order structural controls of the compressibility of individual pyroxenes are thought to be well understood (cf. Thompson and Downs 2004); however, measured pyroxene compressibility systematics are still an area of active research.

Thompson and Downs (2004) hypothesized that clinopyroxene compressibility is largely controlled by the compressive strength of the  $\text{M1O}_6$  chains, which run parallel to  $c$ . These chains of edge-sharing polyhedra derive their compressive strength from short average M-O bonds and small M1-M1 separations. Exami-

nation of the compressibilities of  $\text{Fe}^{3+}\text{O}_6$  vs.  $\text{Fe}^{2+}\text{O}_6$  octahedra in various minerals shows that  $\text{Fe}^{3+}\text{O}_6$  octahedra are significantly stiffer. Details are examined in the discussion section of this paper. The bonds in the  $\text{SiO}_4$  tetrahedra are significantly shorter and therefore stronger than the M-O bonds in the pyroxene structures and the tetrahedra do not compress significantly, nor do they share edges with other polyhedra. This allows each  $\text{SiO}_4$  tetrahedron significant freedom to rotate relative to its neighbors, subject to the constraints of M2-O3 bonds to bridging O atoms (McCarthy et al. 2008). The result is an  $\text{SiO}_4$  tetrahedral chain that, by itself, does not offer significant resistance to compression parallel to the chain. Instead, the tetrahedra rotate, with concomitant kinking of the chains as measured by the O3-O3-O3 angle. The M1 chains cannot respond to compression in a similar manner due to the edge-sharing nature of the polyhedra that make up the chain.

Unit strain ellipsoids represent the three-dimensional shape change of a unit cell, incorporating all influences on compressional behavior. If M1 chains are the major controller of pyroxene compressibility, we might expect the short (i.e., least compressible) axis of the unit strain ellipsoid to lie roughly parallel to the  $\text{M1O}_6$  chain axis ( $\parallel c$ ). However, this is not generally the case. Instead, the short axis of the unit strain ellipsoid in clinopyrox-

\* E-mail: mccarthy.ac@gmail.com

enes typically bisects the *a* and *c* axes,  $\sim 45^\circ$  from *c* (see Fig. 5 in Downs and Singh 2006; cf. Origlieri et al. 2003), demonstrating that there are other significant factors. Thompson and Downs (2008) present a discussion of other controlling factors of pyroxene compression.

Downs (2003) showed that the major differences in pyroxene bond topologies involve M2 bonding. In pyroxenes, M2 is always bonded to at least four O atoms: two O1s and two O2s. In addition, M2 is usually bonded to either one, two, or four O3 atoms. The inset in Figure 1 illustrates the bonding around M2 in aegirine and the atom nomenclature (Downs 2003) used in this paper. The equivalent nomenclature from Burnham et al. (1967) is illustrated in Figure 1 of Thompson and Downs (2008). McCarthy et al. (2008) examined the effects of the various types of M2-O3 bonds on bulk modulus in *C2/c* and *P2<sub>1</sub>/c* pyroxenes. Increasing pressure on pyroxenes increases the kinking of their tetrahedral chains, as shown in numerous high-*P* studies. As T-chains become more kinked, and individual tetrahedra rotate, one of the bridging oxygen atoms (O3) moves closer to M2 than would be expected based simply on scaled contraction of the unit cell, while the other bridging O3 atom in the same chain moves away from M2. Figure 1 illustrates the tetrahedral rotation in aegirine, and the resulting effects on M2-O3 separations. Where M2-O3 bonds are present across these M2-O3 separations, the first type—if they provide no opposition to kinking—are termed “apathetic” (to T-chain kinking). If such bonds facilitated T-chain kinking they would be termed “sympathetic.” In contrast, the third type of M2-O3 bond shortens less than expected when the T-chains kink. In other words, in the absence of compression,

T-chain kinking would lengthen these bonds. This has the effect of opposing tetrahedral rotation; thus these bonds are termed “antipathetic” (to T-chain kinking). Antipathetic and sympathetic/apathetic bond types are illustrated in Figure 4 of McCarthy et al. (2008). It must be noted that all interatomic distances in pyroxenes are observed to decrease with pressure, and that antipathetic M2-O3 bond lengths simply decrease less than expected based on scaling of the unit cell (McCarthy et al. 2008).

McCarthy et al. (2008) plotted bulk moduli vs. ambient (or minimum stability pressure) unit-cell volumes for 19 silicate clinopyroxenes (space groups *C2/c* and *P2<sub>1</sub>/c*). The data show wide dispersion, but the dispersion could be removed by describing two roughly linear trends with *R*<sup>2</sup> values of 0.83 (stiff trend) and 0.91 (soft trend). Close examination of M2-O3 bonding in relation to tetrahedral rotation with pressure revealed that all the structures in the upper, stiff trend exhibited some antipathetic M2-O3 bonds, while the structures in the lower, more compressible or soft trend exhibited no such bonds. Thus it turned out that M2-O3 bonding does impact pyroxene compressibilities, primarily due to its relationship with T-chain kinking.

#### RELATED PREVIOUS WORK ON AEGIRINE

The structure of aegirine—at the time called acmite—was first reported by Clark et al. (1969). The mineral is isostructural with jadeite, NaAlSi<sub>2</sub>O<sub>6</sub>, and kosmochlor, NaCrSi<sub>2</sub>O<sub>6</sub>, other *C2/c* pyroxene group minerals with Na at M2. Aegirine has been the subject of several previous studies at non-ambient conditions: at high temperatures by Cameron et al. (1973) and at high pressure by Nestola et al. (2006) and by Downs and Singh (2006), the latter in a non hydrostatic environment. However, high-pressure structural information (i.e., atomic positions) for aegirine has not been previously reported.

Cameron et al. (1973) examined the aegirine structure at four temperatures from ambient to 800 °C. They found that aegirine cell parameters (*a*, *b*, *c*, β) and average M-O distances (Na-O, Fe-O) increased linearly with temperature. Over the temperature range studied, they observed rather minor changes in the aegirine cell parameters and interatomic angles. For example, a change in the O3-O3-O3 angle of 0.7° [from 174.0(2)° to 174.7(2)°] was observed. In contrast, high-pressure studies such as the present one often reveal an O3-O3-O3 angle change of  $\geq 8^\circ$ .

Downs and Singh (2006) examined data from the same high-pressure experiment discussed in this paper. Their focus was the response of aegirine above 11.55 GPa, caused by the non-hydrostatic freezing of the ethanol:methanol pressure medium.

Nestola et al. (2006) examined four crystals from the jadeite-aegirine solid solution at high pressures. They examined an end-member aegirine crystal over the pressure range 0–9.74 GPa and reported unit-cell parameters at 12 pressures. They reported a bulk modulus of 116.1(5) GPa and its pressure derivative, *K*<sub>0</sub>' = 4.4(1), based on a third-order Birch-Murnaghan fit of their unit-cell data.

#### EXPERIMENTAL METHODS

A pure synthetic aegirine crystal reported in Redhammer et al. (2000), run Nahp2, was selected for study based on crystal quality as determined by examination of peak profiles. Typical peak widths are 0.08° in  $\omega$ . The size of the crystal is  $\sim 115 \times 70 \times 50 \mu\text{m}$ .

Diffraction data were collected with an automated Picker four-circle diffractometer using unfiltered MoK $\alpha$  radiation and operating at 45 kV and 40 mA.

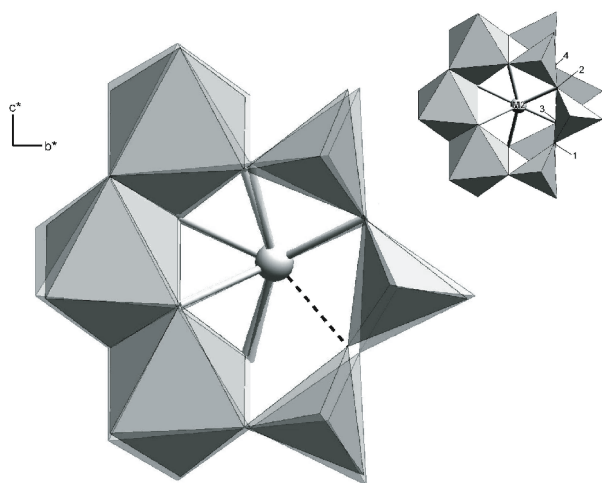


**FIGURE 1.** Superimposed images of the aegirine structure around M2 at ambient pressure and at 10.82 GPa. View is along *a*\*. For clarity, only the top T-chain is shown (contrast with inset). The structure with the more rotated tetrahedra is at 10.82 GPa. The (unbonded) sympathetic/apathetic distance M2-O3<sub>1</sub> is indicated with the dashed line. Note how this sympathetic/apathetic distance decreases visibly with pressure, whereas the bonded M2-O3<sub>2</sub> distance decreases little. These changes are brought about primarily by the rotation of the SiO<sub>4</sub> tetrahedra. The inset figure illustrates the aegirine structure and oxygen atom nomenclature around M2 (Na). The oxygen atoms that bridge the SiO<sub>4</sub> tetrahedra, O3, are numbered 1–4 according to their position relative to M2 (Downs 2003).

**TABLE 1.** Aegirine unit-cell data as a function of pressure

Run	<i>P</i> (GPa)	<i>a</i> (Å)	<i>b</i> (Å)	<i>c</i> (Å)	$\beta$ (°)	<i>V</i> (Å <sup>3</sup> )
P0*	0.0001	9.6539(2)	8.7928(2)	5.2935(2)	107.436(2)	428.69(2)
P1	0.56(3)	9.6406(3)	8.7825(5)	5.2871(2)	107.386(3)	427.20(3)
P2	1.20(3)	9.6221(4)	8.7644(4)	5.2778(2)	107.318(3)	424.91(3)
P3*	1.78(3)	9.6067(3)	8.7501(4)	5.2698(2)	107.258(3)	423.03(2)
P4	2.62(3)	9.5858(4)	8.7307(5)	5.2585(2)	107.171(4)	420.47(3)
P5*	3.35(3)	9.5667(4)	8.7128(5)	5.2484(2)	107.095(4)	418.14(3)
P7*	5.47(3)	9.5148(3)	8.6568(3)	5.2188(3)	106.844(4)	411.42(3)
P7a	6.29(3)	9.4948(2)	8.6364(3)	5.2062(2)	106.757(3)	408.79(2)
P9*	7.30(3)	9.4711(2)	8.6068(3)	5.1915(1)	106.633(2)	405.48(2)
P11	8.09(3)	9.4551(3)	8.5885(4)	5.1815(2)	106.551(3)	403.33(2)
P12*	8.63(3)	9.4426(3)	8.5727(4)	5.1740(2)	106.482(3)	401.62(2)
P13	9.09(3)	9.4342(4)	8.5631(6)	5.1677(3)	106.439(4)	400.41(3)
P14*	9.76(3)	9.4220(2)	8.5480(4)	5.1597(2)	106.371(3)	398.71(2)
P15	10.37(3)	9.4125(3)	8.5342(5)	5.1526(3)	106.314(4)	397.23(3)
P17*	10.82(3)	9.4038(3)	8.5221(5)	5.1465(3)	106.256(4)	395.95(3)
P18	11.55(3)	9.3931(4)	8.5065(6)	5.1394(3)	106.187(4)	394.37(4)

Note: Space group = *C2/c*.

\* Intensity data collected at this pressure.

Before loading in the diamond cell, the crystal was examined in air. The positions of 28 high-intensity peaks ( $13^\circ < 2\theta < 30^\circ$ ) were determined using a modification of the eight-peak centering technique of King and Finger (1979), by fitting both  $K\alpha_1$  and  $K\alpha_2$  profiles with Gaussian functions. Refined cell parameters constrained to monoclinic symmetry are reported in Table 1. A half-sphere of intensity data were collected to  $2\theta \leq 60^\circ$ , using  $\omega$  scans of  $1^\circ$  width, step size  $0.025^\circ$ , and 5 s per step counting times. The structure was refined on *F* with anisotropic displacement parameters using a modification of RFINE (Finger and Prince 1975) to  $R_w = 0.012$ . Structural data at room conditions are summarized in Table 2. These data have smaller errors than Clark et al. (1969) ( $R_w = 0.039$ ), but otherwise compare favorably.

The aegirine crystal was loaded into a four-pin Merrill-Bassett type diamond-anvil cell with beryllium seats, with the (110) face parallel to the culet surfaces. The diamond anvil culet size was 600  $\mu\text{m}$ . A 250  $\mu\text{m}$  thick stainless steel gasket, pre-indented to 100  $\mu\text{m}$ , with a hole diameter of 300  $\mu\text{m}$ , was used. The cell was loaded with the aegirine crystal, a small ruby fragment, and a 4:1 mixture of methanol:ethanol as pressure medium. Ruby fluorescence spectra were collected before and after each collection of intensity data, and the positions of the  $R_1$  and  $R_2$  peaks were determined by fitting with Lorentzian functions. Pressure was calculated from the fitted  $R_1$  and  $R_2$  peak positions using the method of Mao et al. (1978), with an estimated error of  $\pm 0.05$  GPa.

The experiment was carried out under hydrostatic conditions to a pressure of 11.15 GPa. Intensity data were collected at nine pressures. Above this pressure, conditions appeared to be non-hydrostatic due to the freezing of the pressure medium. A discussion of the behavior of aegirine at non-hydrostatic conditions from the same experiment is presented by Downs and Singh (2006).

Every accessible reflection allowed by *C2/c* symmetry, up to 728 intensity data ( $2\theta \leq 60^\circ$ ), were collected at pressure, with  $\omega$  scans of  $1^\circ$  width, in steps of  $0.025^\circ$  and counting times of 10 s per step. These data reduced to 320 inequivalent reflections. Reflections violating *C2/c* were examined, but none with significant intensities were found throughout the experiment. Absorption corrections for the beryllium seats and diamond anvils were made from an absorption correction profile of the diamond cell before loading. Structure factors were weighted by  $w = [\sigma_F^2 + (pF)^2]^{-1}$ , where  $\sigma_F$  was obtained from counting statistics and *p* chosen to ensure normally distributed errors (Ibers and Hamilton 1974). Structure data were refined with isotropic displacement factors using a modified version of RFINE (Finger and Prince 1975) and are summarized in Table 3. Refinements from data collected at pressure yield  $R_w$  values ranging from 0.041 to 0.051.

Bond lengths, angles, and errors were calculated using BOND91 software,

modified after Finger and Prince (1975). Polyhedral volumes and quadratic elongations were obtained with XTALDRAW (Downs and Hall-Wallace 2003). Selected bond lengths, angles, and polyhedral volumes are presented in Table 4.

**RESULTS AND DISCUSSION**

Downs and Singh (2006) report a third-order Birch-Murnaghan *P-V* equation of state fit to measured cell parameters of aegirine from this experiment, over 0–11.15 GPa. This fit resulted in values of  $K_0 = 117(1)$  GPa,  $K'_0 = 3.2(2)$ , and  $V_0 = 429.40(9)$  Å<sup>3</sup>. These values, with the exception of  $K'_0$ , closely correspond to those reported by Nestola et al. (2006) from the pressure range 0–9.74 GPa:  $K_0 = 116.1(5)$  GPa,  $K'_0 = 4.4(1)$ ,  $V_0 = 429.26(2)$  Å<sup>3</sup>. The data and fitted curve from our experiment are plotted in Figure 2. The compressibility of aegirine, as reflected by  $V/V_0$ , is compared to that of other clinopyroxenes in Figure 2 of McCarthy et al. (2008). Aegirine is the most compressible of the Na-clinopyroxenes studied to date (a group that comprises jadeite, kosmochlor, and aegirine). No evidence of a symmetry transformation in aegirine was observed to a pressure of 11.15 GPa. All observed cell parameters decrease continuously with increasing pressure.

Cell-parameter data were used to construct unit strain ellipsoids with STRAIN, modified after Ohashi (1982). The unit strain ellipsoid (see Fig. 5 in Downs and Singh 2006) is highly anisotropic, with axial ratios  $\epsilon_1:\epsilon_2:\epsilon_3$  of 1.00:2.38:2.63 in the range 0–11.55 GPa. The axial values of the unit strain ellipsoid are  $\epsilon_1, -0.001196$ ;  $\epsilon_2, -0.002725$ ; and  $\epsilon_3, -0.003050$  GPa<sup>-1</sup>, with  $\epsilon_3$  oriented  $55.9^\circ$  from *c*, and  $\epsilon_2$  parallel to *b*. Our results are similar to those of Nestola et al. (2006) who report aegirine unit strain ellipsoid axial ratios of 1.00:2.38:2.76 between 0 and ~5 GPa.

Procrystal electron density analysis of aegirine indicates the presence of six Na-O bonds at room conditions (Downs 2003), giving the mineral a bond topology identical to jadeite, kosmochlor, and all other known *C2/c* pyroxenes with Na occupying M2 (Thompson et al. 2005). Na in aegirine resides on a twofold axis, constraining the coordination of Na to an even number, and resulting in three pairs of equivalent Na-O bonds. The bond nomenclature used in this paper is described in Downs (2003) and illustrated in Figure 1. Na is not bonded to two nearest-neighbor O atoms, O<sub>31</sub> and O<sub>34</sub>, found at a distance of 2.834(2) Å at ambient pressure. All Na-O distances in aegirine decrease with pressure, although at different rates (Fig. 3). As in other Na clinopyroxenes, the (unbonded) Na-O<sub>31,4</sub> distance is observed to decrease at a much higher rate [ $dR(\text{NaO})/dP$ ] than the bonded Na-O distances (McCarthy et al. 2008; Origlieri et al. 2003). At a sufficiently high pressure, the unbonded O<sub>31,4</sub> atoms are expected to come close enough to Na at M2 to allow bond formation, making Na 8-coordinated with oxygen and bringing about a *C2/c* → *C2/c* bonding transition. The trend of the

**TABLE 2.** Structural parameters for aegirine in air at room conditions

Atom	<i>x</i>	<i>y</i>	<i>z</i>	$B_{\text{eq}}$ (Å <sup>2</sup> )	$\beta_{11}$	$\beta_{22}$	$\beta_{33}$	$\beta_{12}$	$\beta_{13}$	$\beta_{23}$
NaM2	0	0.2992(1)	¼	1.022(19)	0.00364(14)	0.00275(14)	0.00714(40)	0	-0.00050(19)	0
FeM1	0	0.89878(5)	¼	0.407(8)	0.00119(5)	0.00128(5)	0.00404(14)	0	0.00057(6)	0
Si	0.29072(5)	0.08945(6)	0.23561(8)	0.370(8)	0.00106(5)	0.00132(6)	0.00344(16)	-0.00012(5)	0.00066(8)	-0.00008(9)
O1	0.1143(1)	0.0786(1)	0.1376(2)	0.508(20)	0.00124(12)	0.00187(16)	0.00508(41)	-0.00018(12)	0.00069(19)	-0.00008(21)
O2	0.3588(1)	0.2558(2)	0.3007(2)	0.674(21)	0.00238(15)	0.00170(16)	0.00722(45)	-0.00059(12)	0.00164(21)	-0.00062(21)
O3	0.3520(1)	0.0078(1)	0.0120(3)	0.585(18)	0.00145(12)	0.00241(14)	0.00510(40)	0.00001(13)	0.00081(18)	-0.00077(24)

Note: Space group = *C2/c*.

**TABLE 3.** Structural parameters for aegirine as a function of pressure

P (GPa)	0.0001	1.78	3.35	5.47	7.3	8.63	9.76	10.82
	P0	P3	P5	P7	P9	P12	P14	P17
obs refl	476	220	214	210	214	217	208	200
total refl	624	320	312	295	294	302	298	292
$p^*$	0.004	0.035	0.030	0.040	0.030	0.034	0.037	0.035
$R_w$	0.012	0.047	0.043	0.051	0.041	0.047	0.047	0.046
Fe y	0.89878(5)	0.8997(2)	0.9005(2)	0.9006(2)	0.9014(2)	0.9015(2)	0.9018(2)	0.9021(2)
B	0.407(8)	0.64(4)	0.65(4)	0.58(4)	0.64(3)	0.60(4)	0.82(4)	0.74(4)
Na y	0.2992(1)	0.3002(5)	0.3011(5)	0.3029(5)	0.3044(4)	0.3048(5)	0.3050(5)	0.3059(5)
B	1.02(2)	1.08(8)	1.08(8)	1.11(8)	1.09(7)	0.98(7)	1.17(8)	1.07(8)
Si x	0.29072(5)	0.2904(2)	0.2907(2)	0.2909(3)	0.2911(2)	0.2911(2)	0.2911(2)	0.2916(2)
y	0.08945(6)	0.0901(3)	0.0908(3)	0.0909(2)	0.0917(2)	0.0920(3)	0.0918(3)	0.0922(3)
z	0.23561(8)	0.2355(4)	0.2356(4)	0.2366(5)	0.2365(4)	0.2367(4)	0.2368(4)	0.2377(3)
B	0.370(8)	0.61(4)	0.57(4)	0.54(4)	0.59(3)	0.60(4)	0.77(4)	0.69(4)
O1 x	0.1143(1)	0.1150(7)	0.1150(6)	0.1141(7)	0.1146(6)	0.1135(6)	0.1149(6)	0.1141(6)
y	0.0786(1)	0.0792(6)	0.0800(6)	0.0801(6)	0.0821(5)	0.0827(6)	0.0824(7)	0.0822(7)
z	0.1376(2)	0.1397(10)	0.1398(9)	0.1414(12)	0.1416(9)	0.1411(10)	0.1412(9)	0.1414(9)
B	0.51(2)	0.80(9)	0.68(8)	0.67(9)	0.64(7)	0.70(8)	0.78(8)	0.72(8)
O2 x	0.3588(1)	0.3595(7)	0.3574(6)	0.3573(7)	0.3574(6)	0.3567(6)	0.3562(6)	0.3573(6)
y	0.2558(1)	0.2567(7)	0.2578(6)	0.2602(6)	0.2607(5)	0.2617(6)	0.2615(7)	0.2619(7)
z	0.3007(2)	0.3028(10)	0.3052(10)	0.3081(1)	0.3135(9)	0.3144(10)	0.3186(9)	0.3186(9)
B	0.67(2)	0.90(9)	0.82(9)	0.77(9)	0.83(8)	0.95(9)	0.94(9)	0.96(9)
O3 x	0.3520(1)	0.3527(7)	0.3532(7)	0.3548(7)	0.3549(5)	0.3558(6)	0.3557(6)	0.3564(6)
y	0.0078(1)	0.0107(6)	0.0125(6)	0.0130(6)	0.0156(5)	0.0175(6)	0.0188(7)	0.0192(7)
z	0.0120(3)	0.0110(10)	0.0101(10)	0.0094(1)	0.0058(10)	0.0044(10)	0.0032(9)	0.0032(10)
B	0.59(2)	0.74(9)	0.76(8)	0.72(9)	0.78(7)	0.59(8)	0.98(8)	0.86(9)

Note:  $x_{Fe} = x_{Na} = 0$ ;  $z_{Fe} = z_{Na} = 1/4$ .

\* Weights computed by  $\omega = [\sigma_F^2 + (pF)^2]^{-1}$ .

**TABLE 4.** Selected bond lengths (Å), volumes (Å<sup>3</sup>), and angles (°) from structure refinements

P (GPa)	0.0001*	1.78	3.35	5.47	7.3	8.63	9.76	10.82
	P0	P3	P5	P7	P9	P12	P14	P17
R(SiO1)	1.628(1)	1.612(6)	1.609(6)	1.612(7)	1.604(5)	1.611(6)	1.596(6)	1.604(6)
R(SiO2)	1.599(1)	1.598(6)	1.588(6)	1.597(6)	1.589(5)	1.588(6)	1.586(6)	1.582(6)
R(SiO3a)	1.639(1)	1.631(6)	1.625(5)	1.628(6)	1.625(5)	1.626(5)	1.620(5)	1.621(5)
R(SiO3b)	1.644(1)	1.652(6)	1.655(6)	1.645(6)	1.640(5)	1.641(5)	1.638(5)	1.635(6)
<R(SiO)>	1.627	1.623	1.619	1.620	1.615	1.616	1.610	1.611
V(SiO <sub>4</sub> )	2.2013	2.1836	2.1694	2.1748	2.1524	2.1595	2.1337	2.1364
R(NaO1)	2.393(1)	2.384(6)	2.372(6)	2.362(6)	2.346(5)	2.331(6)	2.334(6)	2.331(7)
R(NaO2)	2.409(1)	2.395(5)	2.388(5)	2.376(7)	2.350(5)	2.346(5)	2.327(5)	2.323(5)
R(NaO3c)	2.432(1)	2.434(7)	2.431(7)	2.406(7)	2.408(6)	2.411(7)	2.415(7)	2.404(7)
R(NaO3d)†	2.834(1)	2.791(6)	2.757(6)	2.713(6)	2.664(5)	2.631(5)	2.612(6)	2.594(6)
diff	0.402	0.357	0.326	0.307	0.256	0.220	0.197	0.190
<R(NaO)>	2.411	2.404	2.397	2.381	2.368	2.363	2.359	2.353
R(FeO1a)	2.113(1)	2.100(6)	2.089(5)	2.067(5)	2.065(4)	2.054(5)	2.053(5)	2.038(6)
R(FeO1b)	2.027(1)	2.031(5)	2.025(5)	2.024(7)	2.017(5)	2.008(5)	2.008(5)	2.004(5)
R(FeO2)	1.931(1)	1.920(6)	1.929(5)	1.911(6)	1.911(4)	1.906(5)	1.915(5)	1.902(6)
<R(FeO)>	2.024	2.017	2.015	2.001	1.998	1.989	1.992	1.982
V(FeO <sub>6</sub> )	10.8534	10.7621	10.7272	10.4915	10.4607	10.3173	10.3665	10.2074
Si-O3-Si	139.37(9)	139.6(5)	138.3(4)	137.3(4)	137.0(3)	136.1(4)	135.9(4)	135.6(4)
O3-O3-O3	174.1(1)	171.9(5)	170.5(4)	170.1(4)	168.2(4)	166.8(5)	165.8(5)	165.5(5)

Notes: The O3a in SiO3a is at [0.352,0.008,0.012]; the O3c in NaO3c is at [0.148,0.508,0.488]; the O1a in FeO1a is at [0.114,1.079,0.138]; diff: length difference between the shortest and longest reported Na-O3 distances.

\* Structure at 0.0001 GPa was refined with anisotropic temperature factors:

† Not bonded.

decreasing Na-O3<sub>1,4</sub> distance certainly suggests this. However, aegirine has a relatively long M2-O3<sub>1,4</sub> distance (McCarthy et al. 2008) and so does not seem an ideal candidate for displaying the C2/c → C2/c bonding transition at the lowest pressure of any Na clinopyroxene. Still, the unbonded Na-O3<sub>1,4</sub> distance in aegirine is projected to decrease to the ambient length of Na-O2 [2.409(1) Å] at 17.9 GPa, functionally identical to the predicted transition pressure of 17.8 GPa in jadeite (McCarthy et al. 2008). It appears that a high-pressure single-crystal X-ray diffraction study on aegirine or jadeite to ~20 GPa should observe a bond transition phenomenon, perhaps similar to the postulated C2/c →

C2/c transition (Chopelas and Serghiou 2002), assuming other bond configurations in the structure remain stable.

The Fe atom in aegirine resides in the octahedral M1 site. It is 6-coordinated with oxygen at all pressures in this study. Fe-O bond lengths decrease systematically with pressure (Fig. 4). The Fe<sup>3+</sup>O<sub>6</sub> octahedron becomes slightly more regular with pressure, with the mean quadratic elongation (Robinson et al. 1971) decreasing from 1.0135 at ambient conditions to 1.0118 at 10.82 GPa.

The O3-O3-O3 angle in aegirine decreases from 174.1(1)° at ambient conditions to 165.5(5)° at 10.82 GPa (Fig. 5). The

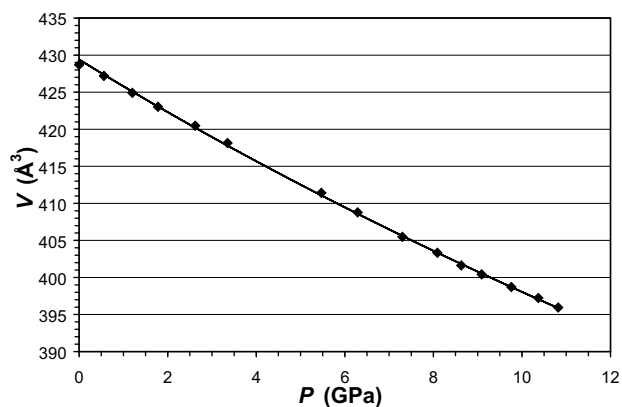


**FIGURE 2.** Unit-cell volume as a function of pressure for aegirine. Data are fit with a third-order Birch-Murnaghan equation with  $V_0 = 429.40(9) \text{ \AA}^3$ ,  $K_0 = 117(1) \text{ GPa}$ , and  $K_0' = 3.2(2)$ . Errors in  $P$  and  $V$  are significantly smaller than the symbols used.

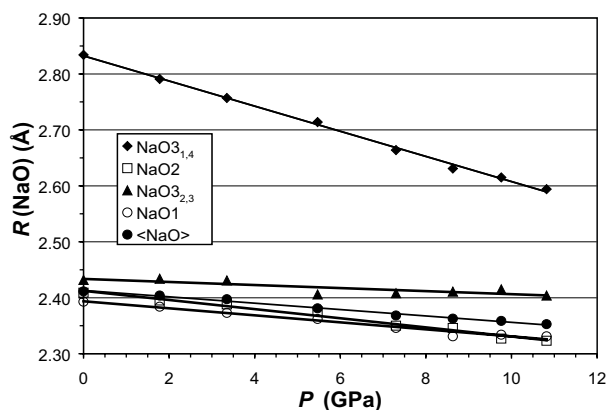
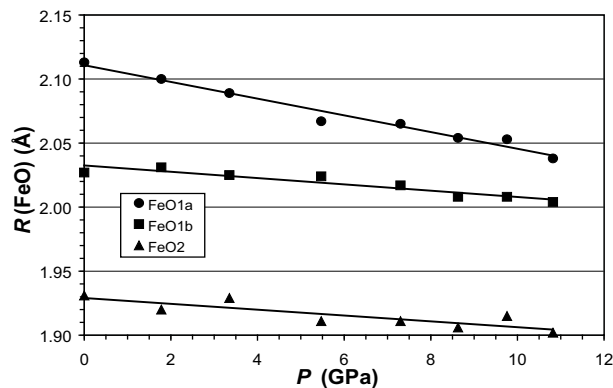


**FIGURE 3.** Variation of Na-O distances in aegirine with pressure at room temperature. Na-O<sub>3,1,4</sub> is the only unbonded pair over the pressure range examined in this study. At a pressure of 17.9 GPa, the linearly extrapolated Na-O<sub>3,1,4</sub> distance is the same as the Na-O<sub>3,2,3</sub> distance at ambient pressure. At this or a lesser pressure, Na-O<sub>3,1,4</sub> bonds may form, making Na 8-coordinated and constituting a  $C2/c \rightarrow C2/c$  bonding transition.

resulting change in the structure due to the decrease in  $\angle O3-O3-O3$  is illustrated in Figure 1. The decrease is approximately linear with  $P$  and the slope ( $d\angle/dP = -0.79^\circ \text{ GPa}^{-1}$ ) generally compares with those of kosmochlor ( $-0.72^\circ \text{ GPa}^{-1}$ ) (Origlieri et al. 2003) and jadeite ( $-0.60^\circ \text{ GPa}^{-1}$ ) (McCarthy et al. 2008). In all three minerals, the silicate tetrahedra become more O-rotated with increased pressure. Model pyroxenes with closest-packed oxygen arrays exhibit O3-O3-O3 angles of  $120^\circ$  (cubic closest packed) and  $240^\circ$  (hexagonal closest packed) (Thompson 1970). Thus the oxygen atoms in aegirine move toward a cubic-closest-packed arrangement with pressure, but they are still far from it at 10.82 GPa.

### M1 size vs. bulk modulus

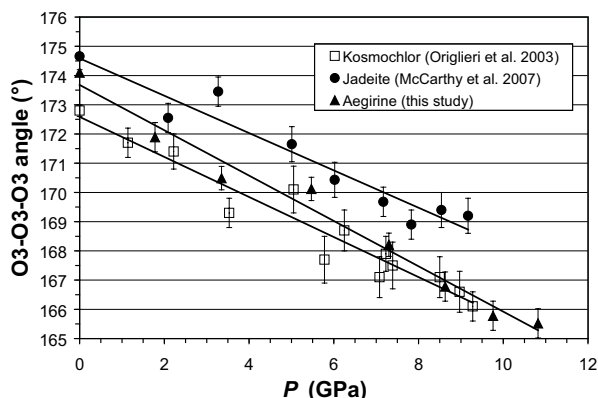
Thompson et al. (2005) demonstrated a near-linear, strongly correlated relationship ( $R^2 = 0.92$ ) between M1 cation radii and unit-cell volumes in a population of 22  $C2/c$  pyroxenes (See



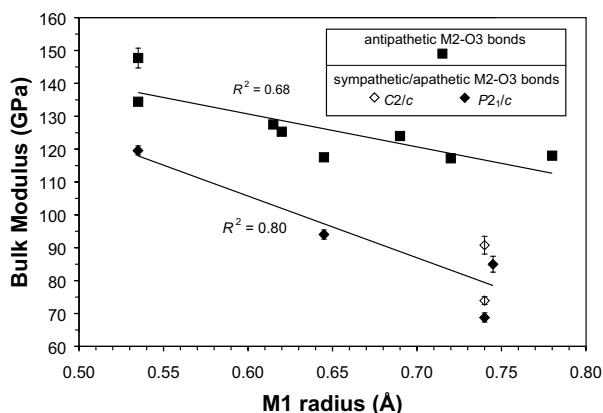
**FIGURE 4.** Variation of Fe-O distances in aegirine with pressure at room temperature.

Fig. 1 in Thompson et al. 2005). The same authors showed that there does not appear to be a linear correlation between M2 cation radius and unit-cell volume. Since bulk moduli are generally correlated with ambient unit-cell volumes in isostructural materials (cf. Bridgman 1923; Anderson and Anderson 1970; Anderson 1972), it follows that the M1 radii and other measures of the M1 polyhedron have a significant effect on determining the clinopyroxene bulk moduli. However, this relationship is too simple to completely explain the variation in clinopyroxene bulk moduli.

In Figure 6, we plot M1 cation radii vs. bulk moduli for 14 clinopyroxene structures (space groups  $C2/c$  and  $P2_1/c$ ) that have been subjected to high-pressure X-ray diffraction studies. (Data used to create Figs. 6 and 7 are presented in Table 5.) Although a general correlation exists between bulk moduli and M1 radii in  $C2/c$  pyroxenes, this relationship is not as robust ( $R^2 = 0.48$ ) as anticipated. This is probably related to the fact that the  $C2/c$  pyroxenes considered are not completely isostructural (i.e., M2-O bonding varies), and therefore do not show identical structural behavior under compression. Unfortunately, our sample population is limited to a subset of the known end-member silicate clinopyroxenes because many have not been subjected to high-pressure X-ray diffraction studies sufficient to allow calculation of reliable bulk moduli. If the pyroxenes are considered based on their M2-O3 bonding topology as described by McCarthy et al. (2008), two trends can be identified in the data, as shown in Figure 6. Pyroxenes with no M2-O3 bonds or M2-O3 bonds that are entirely sympathetic/apathetic, fall on the bottom portion of the figure. A linear fit to this trend yields  $R^2 = 0.80$ . Pyroxenes with some antipathetic M2-O3 bonds fall on the upper portion of the figure. A linear fit to this trend yields  $R^2 = 0.68$ . The dispersion among the trends indicates that structural factors other than the size of the M1 cation, and the details of M2-O3 bonding, influence the compression behaviors of the pyroxenes. For instance, three polymorphs of  $\text{ZnSiO}_3$  are represented in Figure 6. All three fall in the sympathetic/apathetic trend, with M1 (Zn) radius =  $0.74 \text{ \AA}$  (Shannon 1976), and bulk moduli of 69 ( $P2_1/c$ ), 74 (HT  $C2/c$ ), and 91 (HP  $C2/c$ ) GPa (Arlt and Angel 2000). Each polymorph has a distinct M2 bonding topology, which affects the compressibility of the structure, while the M1 cation radius remains constant.



**FIGURE 5.** Variation of  $\angle\text{O3-O3-O3}$  in the Na-clinopyroxenes aegirine, jadeite, and kosmochlor, with pressure at room temperature. Jadeite data from McCarthy et al. (2008); kosmochlor data from Origlieri et al. (2003). Estimated errors in  $P$  are significantly smaller than the symbols used.



**FIGURE 6.** M1 cation radius vs. bulk modulus in  $C2/c$  and  $P2_1/c$  silicate pyroxenes from the literature. The two parameters are poorly correlated, with a linear fit to all the data yielding  $R^2 = 0.48$ . The data are divided into two trends based on M2 bonding geometry.

There are other ways to measure the influence of M1 on the compressibilities of pyroxene structures. Since M1-O distances do vary somewhat in real clinopyroxenes (Fig. 6), an alternate measure of the three-dimensional influence of M1 polyhedra may be its volume. We plot the ambient volume of the M1 polyhedra vs. bulk moduli for the same 14 pyroxenes from the literature (Fig. 7). Again, while the bulk moduli generally increase with decreasing M1 volume, a linear fit to all the data produces a poor correlation ( $R^2 = 0.48$ ). It is clear, therefore, that even though the volumes of the M1 polyhedra vary approximately linearly with the volumes of the pyroxene unit cell (Thompson et al. 2005), and the volumes of the pyroxene unit cell vary approximately linearly with the bulk moduli (when sympathetic/apathetic M2-O3 bonding is taken into account) (McCarthy et al. 2008), the bulk moduli do not vary linearly with the size of M1. Thus, other factors influence the bulk moduli of clinopyroxenes, besides the considered measures of M1 size.

Figure 7 can be split into the same two categories shown in Figure 6: (1) those with antipathetic M2-O3 bonds, and (2) those

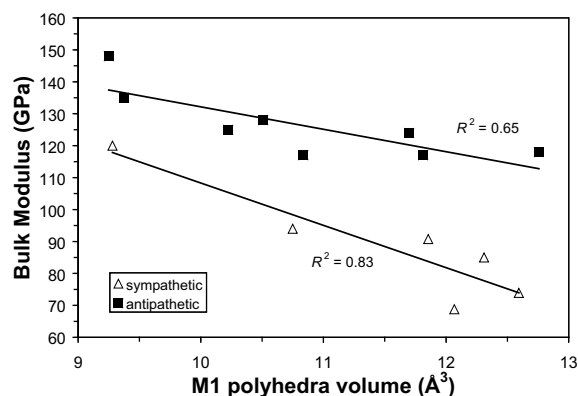


**FIGURE 7.** M1 polyhedral volume vs. bulk modulus in  $C2/c$  and  $P2_1/c$  silicate pyroxenes from the literature. The data are divided into two trends based on M2 bonding topology.

**TABLE 5.** Bulk modulus, cation radius, and polyhedral volume data used to construct Figures 7 and 8

Material	S.G.	$K_0^*$ (GPa)	M1	M1 rad (Å)	M1 poly vol ( $\text{\AA}^3$ )	$P^\dagger$ (GPa)	Ref.
LiAlSi <sub>2</sub> O <sub>6</sub>	$C2/c$	148(3)	Al	0.535	9.250	0.0001	a
NaAlSi <sub>2</sub> O <sub>6</sub>	$C2/c$	134.4(3)	Al	0.535	9.374	0.0001	b
NaGaSi <sub>2</sub> O <sub>6</sub>	$C2/c$	125(1)	Ga	0.620	10.224	0.0001	c
NaCrSi <sub>2</sub> O <sub>6</sub>	$C2/c$	127.5(3)	Cr	0.615	10.509	0.0001	d
NaFeSi <sub>2</sub> O <sub>6</sub>	$C2/c$	117.5(7)	Fe	0.645	10.837	0.0001	e
CaMgSi <sub>2</sub> O <sub>6</sub>	$C2/c$	117.2(3)	Mg	0.720	11.813	0.0001	f
CaFeSi <sub>2</sub> O <sub>6</sub>	$C2/c$	118.0(4)	Fe	0.780	12.757	0.0001	g
CaNiSi <sub>2</sub> O <sub>6</sub>	$C2/c$	124.0(4)	Ni	0.690	11.700	0.0001	h
ZnSiO <sub>3</sub>	$C2/c$	74(1)	Zn	0.740	12.593	0.0001	a
ZnSiO <sub>3</sub>	HP $C2/c$	91(3)	Zn	0.740	11.855	5.05	a
LiAlSi <sub>2</sub> O <sub>6</sub>	$P2_1/c$	120(1)	Al	0.535	9.280	3.19	a
LiFeSi <sub>2</sub> O <sub>6</sub>	$P2_1/c$	94(1)	Fe	0.645	10.750	1.08	i
LiScSi <sub>2</sub> O <sub>6</sub>	$P2_1/c$	85(2)	Sc	0.745	12.310	0.66	a
ZnSiO <sub>3</sub>	$P2_1/c$	69(1)	Zn	0.740	12.067	1.99	a

Notes: Ref. = References: (a) Arlt and Angel (2000); (b) McCarthy et al. (2008); (c) McCarthy et al. (in preparation); (d) Origlieri et al. (2003); (e) Downs and Singh (2006); (f) Thompson and Downs (2008); (g) Zhang et al. (1997); (h) Nestola et al. (2005); (i) Downs et al. (in preparation).

\*  $K_0^*$  constrained to 4.0. See McCarthy et al. (2008) for details on calculation of  $K_0^*$ .

† Minimum pressure of stability of the phase. Pressure ranges are listed in Table 1 of McCarthy et al. (2008).

without. The six pyroxenes on the lower part of Figure 7 have only sympathetic/apathetic bonds, which has the effect of shifting them down on the figure (i.e., they are softer than expected based on the M1 polyhedral volumes). All the other pyroxenes represented have some antipathetic M2-O3 bonds.

### Compression behavior of Fe<sup>2+</sup> vs. Fe<sup>3+</sup> polyhedra

If clinopyroxene compressibilities are controlled to any significant degree by the size of the M1 cation, then those materials with Fe<sup>3+</sup> at M1 should tend to be stiffer than those containing Fe<sup>2+</sup> at this site. The O-O contacts in Fe<sup>3+</sup>O<sub>6</sub> octahedra are shorter than those in Fe<sup>2+</sup>O<sub>6</sub> octahedra, and M1-M1 electrostatic repulsion is stronger for a given M1-M1 separation. Also, Fe<sup>3+</sup>-O bonds are shorter and stiffer than Fe<sup>2+</sup>-O bonds due to the increased electrostatic forces between Fe<sup>3+</sup> and O. Shannon (1976) reports the ionic radii of six-coordinated Fe<sup>2+</sup> and Fe<sup>3+</sup> as 0.780 and 0.645 Å, respectively. The average ambient-condition Fe<sup>2+</sup>-O bond distance in the Fe<sup>2+</sup>O<sub>6</sub> octahedra in hedenbergite is 2.128(1) Å (Zhang et al. 1997), whereas the average Fe<sup>3+</sup>-O bond

in the Fe<sup>3+</sup>O<sub>6</sub> octahedra in aegirine is 2.024(1) Å (this study). The ambient unit-cell volumes of hedenbergite and aegirine are 449.90(7) (Zhang et al. 1997) and 428.69(2) Å<sup>3</sup> (this study). Each one of these factors indicates that aegirine, with Fe<sup>3+</sup> at M1, should be significantly stiffer than hedenbergite, with Fe<sup>2+</sup> at M1. Unexpectedly, however, the compressibilities of the two materials are nearly identical, within two standard deviations, with bulk moduli of 121(2) GPa (hedenbergite, Zhang et al. 1997) and 117(1) GPa (aegirine, Downs and Singh 2006). (All bulk moduli reported herein are recalculated using data from the literature with the constraint that K<sub>0</sub> ≡ 4.0.) It is rather surprising that aegirine does not have a markedly higher bulk modulus than other nearly isostructural pyroxenes with similar ambient unit-cell volumes. Both the aegirine and hedenbergite structures contain antipathetic M2-O3 bonds and thus fall on the upper trend described in McCarthy et al. (2008). Hedenbergite and aegirine are isostructural except for bonding around M2. Procrystal analysis shows that hedenbergite has 8-coordinated Ca while aegirine has 6-coordinated Na in M2 at room conditions (Downs 2003). It is tempting to suggest that this difference in bonding could account for the anomalous stiffness of hedenbergite. However, other C2/c pyroxenes with 8-coordinated Ca at M2 fall on a roughly linear trend (with R<sup>2</sup> = 0.82) with Na clinopyroxenes with bulk modulus plotted vs. ambient unit cell volume (Fig. 9 in McCarthy et al. 2008). The compressibility of the NaO<sub>6</sub> polyhedra compared to that of the CaO<sub>8</sub> polyhedra is considered further, below.

The only other studied silicate clinopyroxene with Fe<sup>3+</sup> at M1 is Li-aegirine (LiFeSi<sub>2</sub>O<sub>6</sub>), which exhibits P2<sub>1</sub>/c symmetry above 1.08 GPa (Hugh-Jones et al. 1997) and has a bulk modulus of 94(1) GPa. This structure contains only sympathetic/apathetic M2-O3 bonds and thus falls on the lower, “soft” trend of McCarthy et al. (2008). Because of this, the LiFeSi<sub>2</sub>O<sub>6</sub> structure is not isostructural with, and thus not directly comparable to, that of aegirine, although the compressibility of the Fe<sup>3+</sup>O<sub>6</sub> octahedra in LiFeSi<sub>2</sub>O<sub>6</sub> is considered below.

To test our assumptions about the comparative compressibilities of the Fe<sup>2+</sup>O<sub>6</sub> and Fe<sup>3+</sup>O<sub>6</sub> octahedra, we identified materials in the literature that contain Fe in octahedral coordination and have been examined with high-pressure single-crystal X-ray diffraction. Polyhedral volumes were derived from reported structures and were fit with a Birch-Murnaghan P-V equation of state in the same manner described above, with K<sub>0</sub> ≡ 4.0. The results from 10 structures containing FeO<sub>6</sub> polyhedra are reported in Table 6. These results show that Fe<sup>3+</sup>O<sub>6</sub> octahedra are stiffer than

Fe<sup>2+</sup>O<sub>6</sub> octahedra, as expected based on polyhedral volumes and average Fe-O bond lengths. Strikingly, the moduli of the Fe<sup>3+</sup>O<sub>6</sub> octahedra in the silicate minerals andradite (Hazen and Finger 1989), aegirine (this study), and Li-aegirine (Downs et al. in preparation) were found to be identical within error: ~150 GPa. However, Fe<sup>3+</sup>O<sub>6</sub> octahedra in the oxide structures of magnetite (Haavik et al. 2000), goethite (Nagai et al. 2003) and Fe<sub>2</sub>O<sub>3</sub> (corundum structure, Sato and Akimoto 1979) exhibit significantly higher moduli: ~220 GPa. A similar dichotomy can be observed among the structures containing Fe<sup>2+</sup>O<sub>6</sub> octahedra. Non-oxide structures exhibit Fe<sup>2+</sup>O<sub>6</sub> polyhedra with bulk moduli ranging from 79(33) GPa (ferrosilite) to 123(3) GPa (hedenbergite). The NaCl-structure oxide FeO contains Fe<sup>2+</sup>O<sub>6</sub> octahedra with a significantly higher modulus: 153(8) GPa.

An approach to compare the relative compressibilities of the various MO<sub>x</sub> polyhedra in the pyroxene structures is to examine normalized polyhedral volumes vs. normalized unit-cell volumes. Such comparisons show which structural units are soft and which are stiff relative to the overall structure. Figures 8a–8e contain such plots for the Fe<sup>3+</sup>-containing minerals aegirine (this study) and Li-aegirine (Downs et al. in preparation), the Fe<sup>2+</sup>-containing mineral hedenbergite (Zhang et al. 1997), in addition to jadeite (McCarthy et al. 2008) and diopside (Thompson and Downs 2008). Several general trends are observed. First, the M1O<sub>6</sub> polyhedra compress relatively less (i.e., they are stiffer) than the overall structure in all the minerals except diopside. This observation agrees with the oft-repeated argument that the M1 polyhedra in pyroxenes provide stiffness to the structure. Conversely, the M2O<sub>x</sub> polyhedra in all of the minerals examined compress more (i.e., they are softer) than the overall structure.

The behavior of both types of MO<sub>x</sub> polyhedra in aegirine is comparable to that of those in jadeite. In both minerals, the NaO<sub>6</sub> polyhedra compress more readily than the overall structure, while the M1<sup>3+</sup>O<sub>6</sub> polyhedra compress less readily. In contrast with aegirine and jadeite, hedenbergite contains M2 polyhedra (CaO<sub>8</sub>), which are only slightly more compressible than the overall structure. Also, the normalized compression of the Fe<sup>2+</sup>O<sub>6</sub> octahedra in hedenbergite closely matches the compression of the unit cell, whereas the Fe<sup>3+</sup>O<sub>6</sub> octahedra in aegirine compress relatively less than the overall structure. To understand why hedenbergite is stiffer than expected, it can be contrasted with the isostructural mineral diopside. The diopside structure exhibits some unusual compression behavior in that both the MgO<sub>6</sub> and the CaO<sub>8</sub> polyhedra compress relatively more (i.e., they are softer) than the overall structure. This indicates that

**TABLE 6.** Compressibilities of Fe<sup>2+</sup>O<sub>6</sub> and Fe<sup>3+</sup>O<sub>6</sub> octahedra in various structures

Material	Ideal formula	FeO <sub>6</sub> K (GPa)	M	V <sub>0</sub>	<M1-O>	Bulk K <sub>0</sub> (GPa)	Reference
Andradite	Ca <sub>3</sub> Fe <sup>3+</sup> (SiO <sub>4</sub> ) <sub>3</sub>	154(4)	Fe <sup>3+</sup>	11.2875	2.038	159(2)	Hazen and Finger (1989)
Aegirine	NaFe <sup>3+</sup> Si <sub>2</sub> O <sub>6</sub>	152(3)	Fe <sup>3+</sup>	10.8534	2.024	117(1)	this study
Li-aegirine	LiFe <sup>3+</sup> Si <sub>2</sub> O <sub>6</sub>	139(12)	Fe <sup>3+</sup>	10.8740	2.025	94(1)	Downs et al. (in prep)
Magnetite	Fe <sup>2+</sup> Fe <sup>3+</sup> O <sub>4</sub>	214(4)	Fe <sup>3+/2+</sup>	11.6078	2.059	217(2)	Haavik et al. (2000)
Goethite	Fe <sup>3+</sup> O(OH)	210(24)	Fe <sup>3+</sup>	10.8470	2.032	111(2)	Nagai et al. (2003)
Fe <sub>2</sub> O <sub>3</sub> (corundum)	Fe <sup>3+</sup> O <sub>3</sub>	231(10)	Fe <sup>3+</sup>	n/r	n/r	231(10)	Sato and Akimoto (1979)
Hedenbergite	CaFe <sup>2+</sup> Si <sub>2</sub> O <sub>6</sub>	123(3)	Fe <sup>2+</sup>	12.7661	2.128	118(1)	Zhang et al. (1997)
FeO (NaCl)	Fe <sup>2+</sup> O	153(8)	Fe <sup>2+</sup>	n/r	n/r	153(8)	Hazen and Finger (1982)
FeGeO <sub>3</sub>	Fe <sup>2+</sup> Ge <sup>4+</sup> O <sub>3</sub>	98(5)	Fe <sup>2+</sup>	12.7872	2.134	107(2)	Hattori et al. (2000)
Ferrosilite	Fe <sup>2+</sup> SiO <sub>3</sub>	79(33)	Fe <sup>2+</sup>	12.7226	2.130	109(1)	Hugh-Jones et al. (1997)

Notes: K<sub>0</sub> ≡ 4.0. n/r = values not reported in reference.

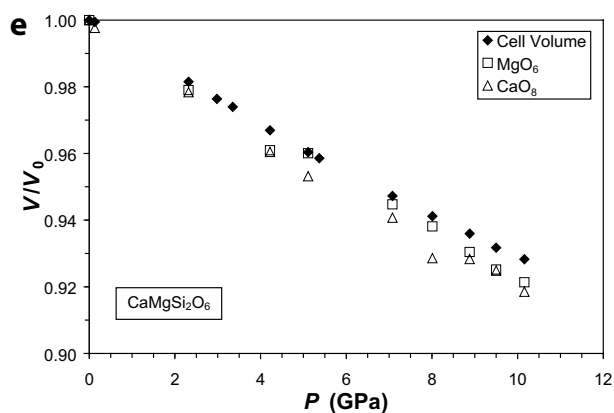
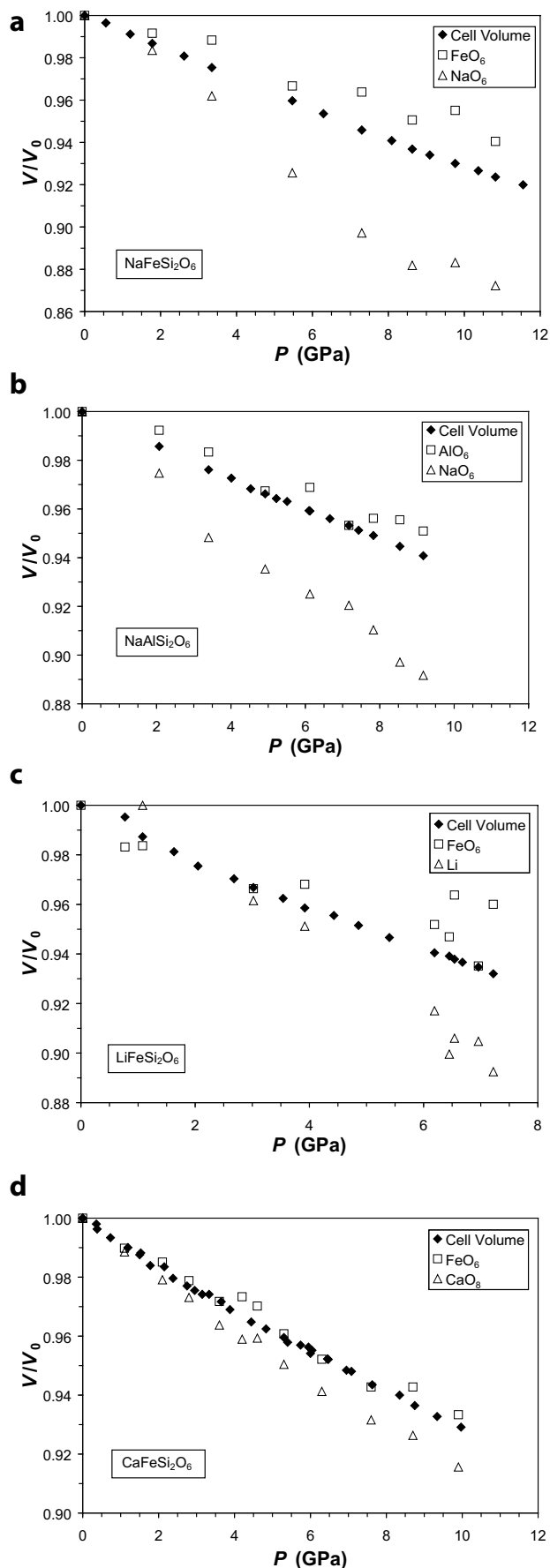


**FIGURE 8.** Normalized unit-cell and M polyhedral volumes from several clinopyroxenes studied at high pressures: (a) aegirine (this study); (b) jadeite (McCarthy et al. 2008); (c) Li-aegirine (Downs et al. in preparation); (d) hedenbergite (Zhang et al. 1997); (e) diopside (Thompson and Downs 2008).

non-polyhedral volumes must be acting to stiffen the structure through interpolyhedral atomic interactions. The important contrast between hedenbergite and diopside is the difference in compression behavior of the M1 octahedra,  $\text{Fe}^{2+}\text{O}_6$  and  $\text{MgO}_6$ . The  $\text{Fe}^{2+}\text{O}_6$  octahedra are stiffer than the  $\text{MgO}_6$  octahedra, lending hedenbergite its anomalously high bulk modulus, considering its ambient unit-cell volume compared to diopside.

#### ACKNOWLEDGMENT

We thank the National Science Foundation for funding our study, Compression Mechanisms of Upper Mantle Minerals, through grant no. EAR-9903104.

#### REFERENCES CITED

- Anderson, D.L. and Anderson, O.L. (1970) The bulk modulus-volume relationship for oxides. *Journal of Geophysical Research*, 75, 3494–3500.
- Anderson, O.L. (1972) Patterns in elastic constants of minerals important to geophysics. In E.C. Robinson, Ed., *Nature of the Solid Earth*, p. 575–613. McGraw-Hill, New York.
- Arlt, T. and Angel, R.J. (2000) Displacive phase transitions in C-centred clinopyroxenes: Spodumene,  $\text{LiScSi}_2\text{O}_6$  and  $\text{ZnSiO}_3$ . *Physics and Chemistry of Minerals*, 27, 719–731.
- Arlt, T., Angel, R.J., Miletich, R., Armbruster, T., and Peters, T. (1998) High-pressure  $P2_1/c-C2/c$  phase transitions in clinopyroxenes: Influence of cation size and electronic structure. *American Mineralogist*, 83, 1176–1181.
- Bindi, L., Downs, R.T., Harlow, G.E., Safonov, O.G., Litvin, Y.A., Perchuck, L.L., Uchida, H., and Menchetti, S. (2006) Compressibility of synthetic potassium-rich clinopyroxene: In situ high-pressure single-crystal X-ray study. *American Mineralogist*, 91, 802–808.
- Bridgman, P.W. (1923) The compressibility of thirty metals as a function of pressure and temperature. *Proceedings of the American Academy of Arts and Sciences*, 58, 165–242.
- Burnham, C.W., Clark, J.R., Papike, J.J., and Prewitt, C.T. (1967) A proposed crystallographic nomenclature for clinopyroxene structures. *Zeitschrift für Kristallographie*, 125, 109–119.
- Cameron, M., Sueno, S., Prewitt, C.T., and Papike, J.J. (1973) High-temperature crystal chemistry of acmite, diopside, hedenbergite, jadeite, spodumene, and ureyite. *American Mineralogist*, 58, 594–618.
- Clark, J.R., Appleman, D.E., and Papike, J.J. (1969) Crystal-chemical characterization of clinopyroxenes based on eight new structure refinements. *Mineralogical Society of America Special Paper*, 2, 31–50.
- Chopelas, A. and Serghiou, G. (2002) Spectroscopic evidence for pressure-induced phase transitions in diopside. *Physics and Chemistry of Minerals*, 29, 403–408.
- Downs, R.T. (2003) Topology of the pyroxenes as a function of temperature, pressure, and composition determined from the procrystal electron density. *American Mineralogist*, 88, 556–566.
- Downs, R.T. and Hall-Wallace, M. (2003) The *American Mineralogist* crystal structure database. *American Mineralogist*, 88, 247–250.

- Downs, R.T. and Singh, A.K. (2006) Analysis of deviatoric stress from nonhydrostatic pressure on a single crystal in a diamond anvil cell: The case of monoclinic aegirine,  $\text{NaFeSi}_2\text{O}_6$ . *Journal of Physics and Chemistry of Solids*, 67, 1995–2000.
- Finger, L.W. and Prince, E. (1975) A system of Fortran IV computer programs for crystal structure computations. U.S. Bureau of National Standards Technical Note 854, 128 p.
- Gatta, G.D., Ballaran, T.B., and Iezzi, G. (2005) High-pressure X-ray and Raman study of a ferrian magnesian spodumene. *Physics and Chemistry of Minerals*, 32, 132–139.
- Haavik, C., Stølen, S., Fjellvåg, H., Hanfland, M., and Hausermann, D. (2000) Equation of state of magnetite and its high-pressure modification: Thermodynamics of the Fe-O system at high pressure. *American Mineralogist*, 85, 514–523.
- Hattori, T., Nagai, T., Yamanaka, T., Werner, S., and Schulz, H. (2000) Single-crystal X-ray diffraction of  $\text{FeGeO}_3$  high-*P* clinopyroxene (*C2/c*) up to 8.2 GPa. *American Mineralogist*, 85, 1485–1491.
- Hazen, R.M. and Finger, L.W. (1982) *Comparative crystal chemistry: Temperature, pressure, composition, and the variation of crystal structure*, 231 p. John Wiley and Sons, New York.
- (1989) High-pressure crystal chemistry of andradite and pyrope: Revised procedures for high-pressure diffraction experiments. *American Mineralogist*, 74, 352–359.
- Hugh-Jones, D.A. and Angel, R.J. (1994) A compressional study of  $\text{MgSiO}_3$  orthoenstatite to 8.5 GPa. *American Mineralogist*, 79, 405–410.
- Hugh-Jones, D.A., Chopelas, A., and Angel, R.J. (1997) Tetrahedral compression in  $(\text{Mg,Fe})\text{SiO}_3$  orthopyroxenes. *Physics and Chemistry of Minerals*, 24, 301–310.
- Ibers, J.A. and Hamilton, W.C. (1974) *International Tables for X-ray Crystallography*, Vol. IV, 366 p. Kynoch Press, Birmingham, U.K.
- King Jr., H.E. and Finger, L.W. (1979) Diffracted beam crystal centering and its application to high-pressure crystallography. *Journal of Applied Crystallography*, 12, 374–378.
- Mao, H.K., Bell, P.M., Shaner, J.W., and Steinberg, D.J. (1978) Specific volume measurements of Cu, Mo, Pd, and Ag and calibration of the ruby  $R_1$  fluorescence pressure gauge from 0.06 to 1 Mbar. *Journal of Applied Physics*, 49, 3276–3283.
- McCarthy, A.C., Downs, R.T., and Thompson, R.M. (2008) Compressibility trends of the clinopyroxenes, and in situ high-pressure single-crystal X-ray diffraction study of jadeite. *American Mineralogist*, 93, 198–209.
- Nagai, T., Kagi, H., and Yamanaka, T. (2003) Variation of hydrogen bonded O···O distances in goethite at high pressure. *American Mineralogist*, 88, 1423–1427.
- Nestola, F., Boffa Ballaran, T., Tribaudino, M., and Ohashi, H. (2005) Compression behavior of  $\text{CaNiSi}_2\text{O}_6$  clinopyroxene: Bulk modulus systematic and cation type in clinopyroxenes. *Physics and Chemistry of Minerals*, 32, 222–227.
- Nestola, F., Boffa Ballaran, T., Liebske, C., Bruno, M., and Tribaudino, M. (2006) High-pressure behaviour along the jadeite  $\text{NaAlSi}_3\text{O}_6$ -aegirine  $\text{NaFeSi}_2\text{O}_6$  solid solution up to 10 GPa. *Physics and Chemistry of Minerals*, 33, 417–425.
- Ohashi, Y. (1982) A program to calculate the strain tensor from two sets of unit-cell parameters. In R.M. Hazen and L.W. Finger, Eds., *Comparative Crystal Chemistry*, 231 p. John Wiley and Sons, New York.
- Origlieri, M.J., Downs, R.T., Thompson, R.M., Pommier, C.J.S., Denton, M.B., and Harlow, G.E. (2003) High-pressure crystal structure of kosmochlor,  $\text{NaCrSi}_2\text{O}_6$ , and systematics of anisotropic compression in pyroxenes. *American Mineralogist*, 88, 1025–1032.
- Redhammer, G.J., Amthauer, G., Lottermoser, W., and Treutmann, W. (2000) Synthesis and structural properties of clinopyroxenes of the hedenbergite  $\text{CaFeSi}_2\text{O}_6$ -aegirine  $\text{NaFeSi}_2\text{O}_6$  solid-solution series. *European Journal of Mineralogy*, 12, 105–120.
- Robinson, K., Gibbs, G.V., and Ribbe, P.H. (1971) Quadratic elongation—quantitative measure of distortion in coordination polyhedra. *Science*, 172, 567–570.
- Sato, Y. and Akimoto, S. (1979) Hydrostatic compression of 4 corundum-type compounds:  $\alpha\text{-Al}_2\text{O}_3$ ,  $\text{V}_2\text{O}_3$ ,  $\text{Cr}_2\text{O}_3$ , and  $\alpha\text{-Fe}_2\text{O}_3$ . *Journal of Applied Physics*, 50, 5285–5291.
- Shannon, R.D. (1976) Revised effective ionic radii and systematic studies of interatomic distances in halides and chalcogenides. *Acta Crystallographica*, A32, 751–767.
- Thompson, J.B. (1970) Geometric possibilities for amphibole structures: model biopyriboles. *American Mineralogist*, 55, 292–293.
- Thompson, R.M. and Downs, R.T. (2004) Model pyroxenes II: Structural variation as a function of tetrahedral rotation. *American Mineralogist*, 89, 614–628.
- (2008) The crystal structure of diopside at pressure to 10 GPa. *American Mineralogist*, 93, 177–186.
- Thompson, R.M., Downs, R.T., and Redhammer, G.J. (2005) Model pyroxenes III: Volume of *C2/c* pyroxenes at mantle *P*, *T*, and *x*. *American Mineralogist*, 90, 1840–1851.
- Tribaudino, M., Prencipe, M., Bruno, M., and Levy, D. (2000) High-pressure behavior of Ca-rich *C2/c* clinopyroxenes along the join diopside-enstatite ( $\text{CaMgSi}_2\text{O}_6$ - $\text{Mg}_2\text{Si}_2\text{O}_6$ ). *Physics and Chemistry of Minerals*, 27, 656–664.
- Yang, H., Finger, L.W., Pamela, C.G., Prewitt, C.T., and Hazen, R.T. (1999) A new pyroxene structure at high pressure: Single-crystal X-ray and Raman study of the *Pbcn-P2<sub>1</sub>cn* phase transition in protopyroxene. *American Mineralogist*, 84, 245–256.
- Zhang, L., Ahsbahs, H., Hafner, S.S., and Kutoglu, A. (1997) Single-crystal compression and crystal structure of clinopyroxene up to 10 GPa. *American Mineralogist*, 82, 245–258.

MANUSCRIPT RECEIVED JUNE 23, 2007

MANUSCRIPT ACCEPTED MAY 28, 2008

MANUSCRIPT HANDLED BY G. DIEGO GATTA